

## Microwave transmission through a two-dimensional, isotropic, left-handed metamaterial

R. A. Shelby,<sup>a)</sup> D. R. Smith, S. C. Nemat-Nasser, and S. Schultz

*Department of Physics, University of California, San Diego, La Jolla, California 92093-0350*

(Received 24 October 2000; accepted for publication 20 November 2000)

We present experimental data, numerical simulations, and analytical transfer-matrix calculations for a two-dimensionally isotropic, left-handed metamaterial (LHM) at X-band microwave frequencies. A LHM is one that has a frequency band with simultaneously negative  $\epsilon_{\text{eff}}(\omega)$  and  $\mu_{\text{eff}}(\omega)$ , thereby having real values of index of refraction and wave vectors, and exhibiting extended wave propagation over that band. Our physical demonstration of a two-dimensional isotropic LHM will now permit experiments to verify some of the explicit predictions of reversed electromagnetic-wave properties including negative index of refraction as analyzed by Veselago [Usp. Fiz. Nauk **92**, 517 (1964), Sov. Phys. Usp. **10**, 509 (1968)]. © 2001 American Institute of Physics. [DOI: 10.1063/1.1343489]

Recently, Smith *et al.*<sup>1</sup> demonstrated a left-handed metamaterial (LHM), and discussed the relationship of this material to the theoretical predictions of Veselago.<sup>2</sup> Veselago predicted that materials with simultaneous negative effective permittivity  $\epsilon_{\text{eff}}(\omega)$  and negative effective permeability  $\mu_{\text{eff}}(\omega)$  have unusual reversed electromagnetic-wave propagation phenomena. Since the initial report<sup>1</sup> was based on a physical construction of elements which exhibited left-handed propagation for only one dimension (i.e., one direction of incidence and polarization), there remained a critical need to develop and verify that higher-dimensional LHMs could readily be made, so as to provide realistic model systems for confirming the expected reversals of Snell's law, the Doppler shift, and Cherenkov radiation.<sup>2</sup> Here, we provide an experimental demonstration and numerical confirmation that we have now made a two-dimensional (2D) LHM suitable for further experiments that will illustrate some of the predicted reversed electromagnetic properties.

Electromagnetic waves will only propagate in a medium that has a real index of refraction,  $n_{\text{eff}}(\omega) = \sqrt{\epsilon_{\text{eff}}(\omega)\mu_{\text{eff}}(\omega)}$ . If either  $\epsilon_{\text{eff}}(\omega)$  or  $\mu_{\text{eff}}(\omega)$  is negative, then  $n_{\text{eff}}(\omega)$  is imaginary, and there will be no transmission through a thick sample. If, however, both  $\epsilon_{\text{eff}}(\omega)$  and  $\mu_{\text{eff}}(\omega)$  are less than zero, electromagnetic waves will propagate through the medium, but the negative root must be chosen for  $n_{\text{eff}}(\omega)$ ,<sup>3</sup> and the group and phase velocities will be antiparallel.<sup>2</sup>

The initial transmission experiments by Smith *et al.*<sup>1</sup> were performed on a one-dimensional (1D) LHM that consisted of an array of unit cells, each cell consisting of one split-ring resonator (SRR), as discussed by Pendry *et al.*,<sup>4</sup> and one conducting post. The composite displayed an anisotropic left-handed transmission band from 4.70 to 5.15 GHz. These previous experiments were carried out in a 2D scattering chamber described in detail in Ref. 5. As the scattering chamber was originally designed for X-band microwave frequencies (8–12 GHz), we have now changed the design parameters of our material to result in a LHM at X band, and

we are thus able to use X-band waveguide components to couple to the 2D scattering chamber. This allows us to utilize plane-wave incident and transmitted waves, which can be compared more easily to the numerical simulations.

We scaled our transmission band to X-band frequencies by reducing the overall dimensions of the SRRs and achieved 2D isotropy by placing the SRRs along two orthogonal axes in a lattice. To further ease the burden of fabrication, the negative permittivity medium has been introduced as wire strips mounted behind the SRRs. Since the wire strips are much thinner than the posts used in the previous work, it was necessary to increase the density of the wire strips to two per unit cell to achieve similar negative values of the permittivity.

Using a shadow mask/etching technique, we fabricated printed circuit boards with SRRs on one side and wire strips on the other. Figure 1(a) shows a diagram of a single SRR of the type we used for these experiments. The boards were cut and assembled such that each unit cell has six SRRs and two wire strips arranged as shown in Fig. 1(b). The printed circuit board material is 0.25 mm G10 fiberglass and the SRRs and wire strips are 0.03-mm-thick copper. The dielectric

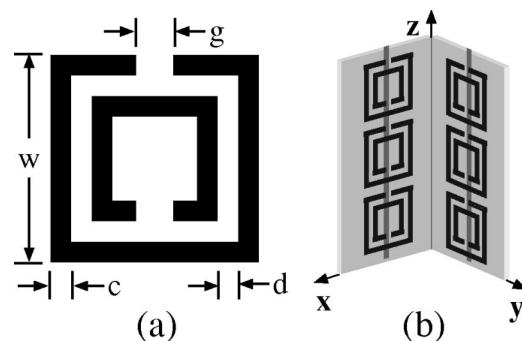


FIG. 1. (a) Diagram of a single split-ring resonator (SRR),  $c=0.25$  mm,  $d=0.30$  mm,  $g=0.46$  mm,  $w=2.62$  mm, and the SRR is square. (b) Each unit cell has six copper SRRs and two wire strips on thin fiberglass boards. The wire strips are 1 cm long, centered on the SRRs, and on the opposite side of the board from the SRRs. The angle between the fiberglass boards is  $90^\circ$  to make square unit cells with a lattice constant of 5.0 mm.

<sup>a)</sup>Electronic mail: rshelby@ucsd.edu

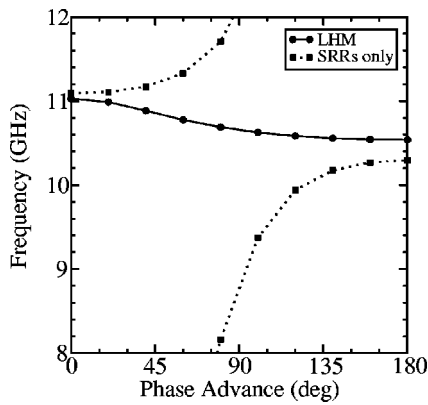


FIG. 2. Numerically simulated dispersion curves for the LHM and “SRR only” material. Notice that the solid curve has a negative slope ( $d\omega/dk < 0$ ). The lower, dotted curve continues to zero frequency at zero-phase advance.

constant of the fiberglass at 10 GHz was measured by placing a piece of the fiberglass into a  $TE_{102}$  X-band microwave cavity and measuring the shift of the cavity’s resonant frequency. The frequency shift of the cavity was simulated for samples with dielectric constants ranging from  $\epsilon_0$  to  $10\epsilon_0$  using the numerical electromagnetic-mode solver called GDFIDL.<sup>6</sup> The measured value of  $(3.4 \pm 0.4)\epsilon_0$  was used in subsequent simulations to obtain the dispersion relations for the LHM.

Figure 2 shows dispersion curves that were numerically simulated with GDFIDL, in the same manner as in Ref. 1. The phase advance  $\phi$  is linearly proportional to the wave number,  $k = (\pi\phi)/(180^\circ a)$ , where  $\phi$  is in degrees and  $a$  is the lattice constant. From the dispersion curve for the “SRRs only” material (not coupled with the wire strips), it can be seen that the simulations predict a forbidden band of frequencies (10.3–11.1 GHz). This is the region corresponding to a negative  $\mu_{\text{eff}}$ . The “wire strips only” (data not shown) has a forbidden frequency band that extends outside the negative  $\mu_{\text{eff}}$  band. Putting the SRRs and wire strips together yields the solid dispersion curve in Fig. 2, indicating a transmission band that has a negative group velocity ( $d\omega/dk$ ). A negative group velocity is one of the necessary characteristic signatures of a LHM.

To perform transmission experiments, the LHM was placed into a 2D microwave-scattering chamber that consists of two large aluminum plates separated by 1 cm, and X-band waveguide input and output ports. The transmission spectrum was measured by introducing microwaves from a Hewlett-Packard 8350B sweep oscillator into one end of the scattering chamber and measuring the transmitted power at the other end of the chamber with a Hewlett-Packard 8756A scalar network analyzer. To test for material isotropy, the transmission spectrum was measured as a function of rotation of the sample, along the [10], [11], and [01] directions, where the rotation axis was the  $z$  axis in Fig. 1(b). The transmission spectra of the LHM for the three orientations is shown in Fig. 3 and “SRRs only” transmission is shown with the [10] data in Fig. 4. Because the resonant frequency of the SRRs is very sensitive to small changes in parameters, a slight systematic misalignment accounts for the shift in the peak frequency of the transmission band.

We also fabricated and performed transmission experi-

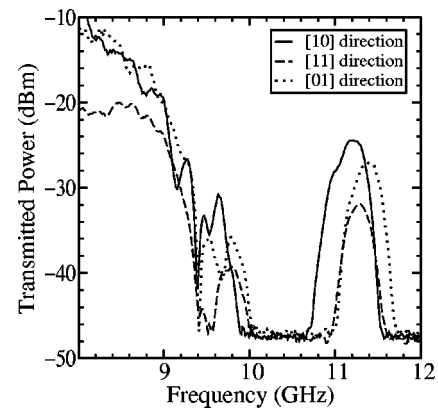


FIG. 3. Experimental data for the 2D LHM in a scattering chamber at different orientations. The sample was a square lattice with 30 unit cells in each direction.

ments on a “wire strips only” material (data not shown) and a “SRRs only” material with all other parameters as close to the original LHM as possible. The transmission data for the “SRRs only” material shows the forbidden band of frequencies at approximately the same frequencies as the numerical simulations predict. A negative  $\mu_{\text{eff}}$  accounts for this lack of transmission, and analytical calculations suggest that  $\mu_{\text{eff}}$  follows the form:<sup>4</sup>

$$\mu_{\text{eff}}(\omega) = 1 - \frac{\omega_{\text{mp}}^2 - \omega_{m0}^2}{\omega^2 - \omega_{m0}^2 + i\gamma\omega}, \quad (1)$$

where  $\omega_{m0}$  is the low-frequency edge of the magnetic forbidden band and  $\omega_{\text{mp}}$  is the “magnetic plasma frequency.” The generic form of the effective permittivity for arrays of wires has also been previously studied and shown to have the form<sup>7</sup>

$$\epsilon_{\text{eff}}(\omega) = 1 - \frac{\omega_{\text{ep}}^2 - \omega_{e0}^2}{\omega^2 - \omega_{e0}^2 + i\gamma\omega}, \quad (2)$$

where  $\omega_{e0}$  is the low-frequency edge of the electrical forbidden band and  $\omega_{\text{ep}}$  is the electric plasma frequency. When the wires maintain electrical continuity,  $\omega_{e0} = 0$ .

With the wire strips attached to the fiberglass boards, it was difficult to maintain electrical connectivity between the strips and the bounding metal surfaces of the scattering chamber. When breaks are introduced into the wires, the result is to introduce a resonant frequency  $\omega_{e0}$  into the permit-

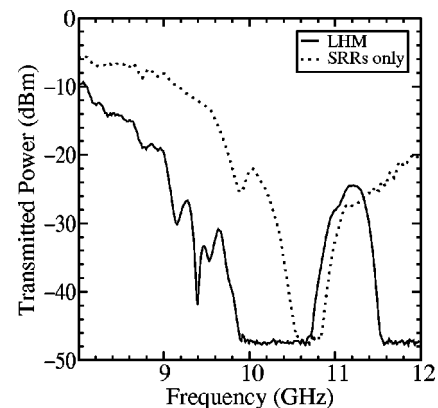


FIG. 4. Experimental transmission data along the [10] direction for the LHM and the “SRR only” material.

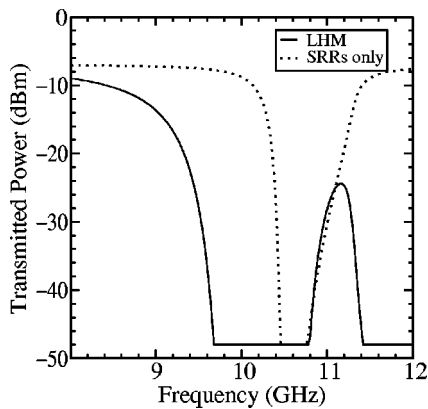


FIG. 5. Transfer-matrix calculation results for the LHM and “SRR only” material.

tivity function<sup>8</sup> as in Eq. (2), thereby reducing the region of negative permittivity to occupy a band between the resonant frequency  $\omega_{e0}$  and the plasma frequency  $\omega_{ep}$ .

The general form of the transmission curves can be compared with a 1D transfer-matrix calculation, assuming the forms in Eqs. (1) and (2) for the material parameters. The results of this calculation, which utilized the method outlined in Ref. 5, are shown in Fig. 5. The following values were used:  $f_{mp} = 11.0$  GHz,  $f_{m0} = 10.5$  GHz,  $f_{ep} = 20$  GHz,  $f_{e0} = 10$  GHz, and  $\gamma = 1$  GHz. The length of the 1D slab was 15 cm. No attempt was made to actually fit the transfer-matrix results to the measured data to derive exact values for the parameters. There is, however, qualitative agreement between the measured and calculated transmitted power curves. Note that the gap due to the negative permeability appears to occur at lower frequency than the transmission band when the negative permittivity is added. This feature is related to the finite size of the structure; the region of negative perme-

ability actually extends to higher frequency, but the associated attenuation length in the material increases such that more power is transmitted through the structure. To match the measured attenuation of the propagation band we set  $\gamma = 1$  GHz, suggesting this structure has relatively large losses.

The agreement between the transfer-matrix calculation and the measured transmittance through the LHM indicates that it is appropriate to treat the LHM as a homogeneous material with frequency-dispersive material parameters. This reduction in complexity is essential to the further interpretation of the LHM concept.

The authors thank Andrew Gray for assistance in assembling the LHMs. This research was supported by DARPA through a grant from ONR (Contract No. N00014-00-1-0632) and by AFOSR (Grant No. F49620-00-1-0380). This research was also supported in part by NSF Cooperative Agreement No. ACI-9619020 through computing resources provided by the National Partnership for Advanced Computational Infrastructure at the San Diego Supercomputer Center.

<sup>1</sup>D. R. Smith, W. Padilla, D. Vier, S. Nemat-Nasser, and S. Schultz, *Phys. Rev. Lett.* **84**, 4184 (2000).

<sup>2</sup>V. G. Veselago, *Usp. Fiz. Nauk* **92**, 517 (1964); *Sov. Phys. Usp.* **10**, 509 (1968).

<sup>3</sup>D. R. Smith and N. Kroll, *Phys. Rev. Lett.* **85**, 2933 (2000).

<sup>4</sup>J. B. Pendry, A. Holden, D. Robbins, and W. Stewart, *IEEE Trans. Microwave Theory Tech.* **47**, 2075 (1999).

<sup>5</sup>D. R. Smith, R. Dalichaouch, N. Kroll, S. Schultz, S. McCall, and P. Platzman, *J. Opt. Soc. Am. B* **10**, 314 (1993).

<sup>6</sup>W. Bruns, *Computer Code GdfidL* (Technische Universität Berlin, Germany, 2000), Version 1.2.

<sup>7</sup>J. B. Pendry, A. Holden, W. Stewart, and I. Youngs, *Phys. Rev. Lett.* **76**, 4773 (1996).

<sup>8</sup>D. F. Sievenpiper, E. Yablonovitch, J. Winn, S. Fan, P. Villeneuve, and J. Joannopoulos, *Phys. Rev. Lett.* **80**, 2829 (1998).